Analysis of the Colorless Operation of a Calibrated 120° Coherent Receiver

David Izquierdo, Jesús Clemente, Pedro J. Reyes-Iglesias, Alejandro Ortega-Moñux, José A. Altabás, Iñigo Molina-Fernández, J. Gonzalo Wangüemert-Pérez, José de Oliva-Rubio, and Ignacio Garcés

***Abstract*— The performance of an integrated InP 120° coherent receiver has been experimentally analyzed using 50 Gbps 16-QAM signals. IQ components are obtained through a set of coefficients applied to the three output photocurrents of the device. It is demonstrated that the calibration of these coefficients can compensate, without extra computational cost, fabrication hardware impairments and allows a wide optical bandwidth (up to 80 nm range) with a high interfering rejection capability. It has been experimentally verified colorless operation in the complete C-band for a received interfering power close to 11 dB above the signal level. This confirms a remarkable colorless behavior of our proposal.**

***Index Terms*— Coherent optical communications, integrated optics, optical communication, optical receivers, photonic integrated circuits**

I. Introduction

RECENTLY, optical networks have increased both their flexibility, by implementing reconfigurable optical add/drop multiplexers (ROADMs), and their capacity, by adopting spectrally-efficient multilevel modulation formats in combination with Dense Wavelength Division Multiplexing (DWDM) systems [1]. In this scenario, the colorless operation of coherent receivers, i.e. the use of these receivers for different signal wavelengths operating in a DWDM scheme, is a relevant issue. Coherent receivers are designed and fabricated for a specific wavelength, but they should operate for a wide range of wavelengths and, at the same time, avoid interference from nearby wavelength channels [2]. They operate by tuning a local oscillator (LO) next to the desired channel to obtain the signal without the use of any additional optical filtering device (e.g. demultiplexer or filter) because the interference of the LO with other channels will be mainly out of the electrical bandwidth of the receiver. Any fabrication defect of the device, including its operation out of the design wavelength, which can be treated as a defect from its theoretical performance, will introduce unwanted signals from other wavelengths into the bandwidth of the receiver. Therefore, a high common-mode rejection ratio (CMRR) of the coherent receiver is required to avoid the unwanted interference due to these fabrication defects and from the nearby channels for any signal wavelength within the optical bandwidth of the device [3].

In conventional coherent receivers, based on 90° optical hybrids and balanced photodetectors to obtain in-phase and quadrature (IQ) signal components, the common-mode will be cancelled only if the power imbalance between the different optical paths of is rather low (i.e. the CMRR is high) [4]. The main drawback of this approach is that stringent fabrication tolerances (resulting in high cost and low fabrication yield) are required to reduce hardware unbalances causing constellation distortion and CMRR degradation. Although constellation distortion can be partially alleviated by complex digital signal processing (DSP) [5], CMRR degradation cannot be solved by using conventional DSP algorithms [6, 7], thus limiting the colorless operation of the 90° receiver with balanced detection. A potentially cost-effective alternative is the coherent receiver based on 120° optical hybrids [6-9]. Although solutions made with fiber components, as symmetric 3×3 fiber couplers and single-ended photodetectors, have successfully demonstrated colorless reception [8], being a non-integrated solution, they do not meet the size and stability constraints required in current state-of-the-art applications. These drawbacks can be overcome using monolithically integrated receivers based on 2×3 multimode interferometer (MMI) 120° hybrids. Compared with conventional 90° hybrids, monolithically integrated 120° optical hybrids exhibit wider optical bandwidth performance and reduced chip size, in conjunction with a simpler design based on three single-ended detectors [6, 7, 9]. As it is well known, realistic receivers can suffer from hardware imbalances between different ports, caused by non-ideal fabrication processes, that give rise to degradations in their performance. Without a proper calibration process, fabrication impairments could significantly reduce the fabrication yield, thus cutting off the potential advantages of integrated solutions [7]. In this work we experimentally demonstrate the potential of the calibration procedure outlined in [7] by applying it to a single-polarization monolithically integrated 120° coherent receiver with

Manuscript submitted October 9, 2020. This work was supported in part by the funds provided by Ministerio de Economía, Industria y Competitividad (TEC2017-85752-R, TEC2016-80718-R); Diputación General de Aragón (T20_17R) and Centro Universitario de la Defensa (UZCUD2019-TEC-01, CUD2019-10).

David Izquierdo is with Centro Universitario de la Defensa, Academia General Militar, Carretera de Huesca, s/n, Zaragoza, 50090, Spain (e-mail: d.izquierdo@unizar.es).

Jesús Clemente and Ignacio Garcés are with Aragon Institute of Engineering Research (I3A), Universidad de Zaragoza, Calle Mariano Esquillor, Edificio I+D+i, Zaragoza, 50018, Spain (e-mail: ngarces@unizar.es).

Pedro J Reyes-Iglesias, Alejandro Ortega-Moñux, Iñigo Molina-Fernández, Gonzalo Wangüemert-Pérez and José de Oliva-Rubio are with Dpto. Ingeniería de Comunicaciones, ETSI Telecomunicación, Universidad de Málaga, Málaga, 29071, Spain (e-mail: reyes@ic.uma.es).

José A. Altabás is with Bifrost Communications, Scion DTU, Kgs Lyngby, Denmark (e-mail: jan@bifrostcommunications.com).

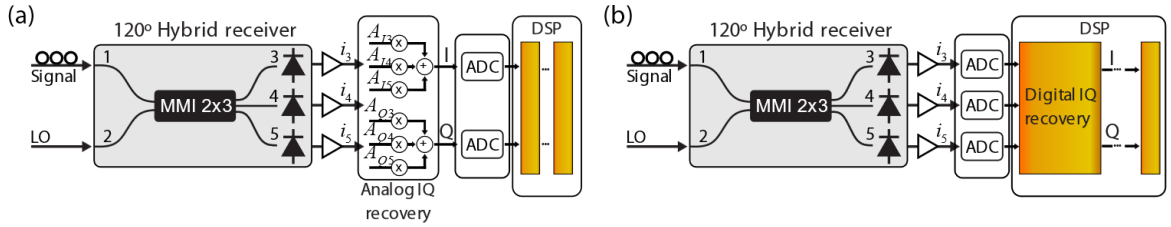

Fig. 1. Schemes of two architectures for 120° phase diversity receiver. Demodulation of IQ signal components is performed from the linear combination of its three photocurrents from (a) analog IQ recovery circuit (b) digital IQ recovery block.

significant hardware impairments. The performance of the calibrated receiver has been experimentally analyzed using 50 Gbps, 16-QAM signals, clearly showing the improvement in both CMMR and adjacent channel interference rejection (i.e., colorless operation). To the best of the authors' knowledge, this is the first experimental demonstration of how an efficient calibration procedure can significantly improve the performance of an integrated receiver with noticeable imbalances, since in previous works the receiver hardware were nearly-ideal and no calibration procedures were required [8, 9].

II. Theory

The aim of a coherent receiver is to determine the polarization, amplitude and phase of an optical signal. This receiver comprises a polarization diversity network (e.g. polarization beam splitters) and two phase diversity downconverters (one per polarization). In this paper we will focus on the last part, that is, the optical downconverter, where the signal is combined with a LO in an optical hybrid. A widely used solution is the 90° hybrid based downconverter, which can be monolithically integrated with a 2×4 MMI (multimode interference) coupler with two pairs of balanced photodiodes followed by transimpedance amplifiers (TIA) [4]. An alternative is a 120° hybrid receiver, based on a 2×3 MMI integrated with three singled-ended photodiodes followed by their respective TIAs, as Fig. 1 depicts assuming a polarization control scenario. The noise analysis carried out in [6] under an ideal hardware implementation showed the same performance for both the 90° and 120° hybrid downconverters, being the common mode noise (e.g. relative intensity noise from LO and signal, Amplified Spontaneous Emission (ASE)-signal, or ASE-ASE beat noise) equally cancelled. Further, the 120° receiver is an attractive solution because, as it is known from multiport theory [10], three is the minimum number of power outputs to perfectly recover IQ signals under hardware impairments by linear means, and thus this is the simplest receiver. In this way, 120° based downconverters are the simplest receivers, further providing a reduction on the chip size, exhibiting a wider optical bandwidth and a greater tolerance to fabrication errors [6, 11].

As it was demonstrated in [7], in the event of a multichannel transmission with the LO tuned to a given channel wavelength, each photocurrent will include the required LO-signal power-dependent combination of the IQ components and an interfering direct-detection term from the self-beating of the adjacent channels. The demodulated IQ signal components can be obtained from the three detected photocurrents (i_j, j = 3, 4 and 5), while cancelling the interfering term from simple linear operations with matrix coefficients (A_{Ij}, A_{Qj}):

$$\begin{bmatrix} I \\ Q \end{bmatrix} = \begin{bmatrix} A_{I3} & A_{I4} & A_{I5} \\ A_{Q3} & A_{Q4} & A_{Q5} \end{bmatrix} \cdot \begin{bmatrix} i_3 \\ i_4 \\ i_5 \end{bmatrix} = \overline{\overline{A}} \cdot \begin{bmatrix} i_3 \\ i_4 \\ i_5 \end{bmatrix}. \quad (1)$$

Under ideal conditions, this colorless operation can be achieved from theoretical coefficients that can be easily calculated [6]:

$$\overline{\overline{A}}_{\substack{Theoretical \\ coefficients}} = \begin{bmatrix} -\frac{1}{2} & 1 & -\frac{1}{2} \\ \frac{\sqrt{3}}{2} & 0 & -\frac{\sqrt{3}}{2} \end{bmatrix}. \quad (2)$$

In a realistic fabrication scenario, it will be necessary to introduce calibrated coefficients to overcome hardware impairments and recover the transmitted symbol constellation. This calibration can be carried out at a unique wavelength (for example at the middle of the operation band) by applying a least squares adjustment to the three output photocurrents with a group of known transmitted symbols [6]. Although the undistorted IQ demodulation and interfering rejection are theoretically obtained at that unique wavelength, the nearly-ideal receiver performance and the wider fabrication tolerance of the 2×3 MMI will allow simple and efficient extraction of IQ components for any channel in a wideband spectrum with the same coefficients [7]. A wider operation band could even be covered using a lookup table with calibrated coefficients obtained at intermediate wavelengths. In this way, the calibrated 120° receiver could operate in any of the S, C or L bands.

As Fig.1 shows, this extraction of IQ components (1) can be performed analogically (Fig. 1.a) or digitally (Fig. 1.b), respectively. It should be highlighted that the analog IQ recovery option has important advantages with respect to the digital approach [7] because: i) it requires one analog-to-digital converter (ADC) less and ii) the interfering direct-detection term is largely cancelled prior to the ADC conversion without reducing its effective number of bits (ENoB).

Conventional receivers based on 90° hybrids with balanced photodetection can be conditioned to a limited operation band

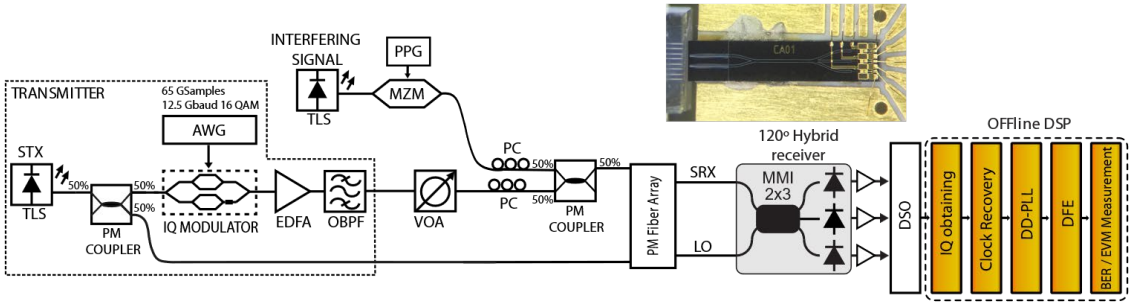

Fig. 2. Experimental setup for characterizing the integrated 120° downconverter receiver.

or stringent fabrication requirements to reduce the amplitude and phase imbalances responsible of distorted IQ constellation and CMRR degradation [7, 11]. The figure of merit to evaluate the colorless behavior of the receiver is the CMRR, as any change in the operation wavelength or introduction of different wavelengths in the optical hybrid will give rise to amplitude imbalances in the balanced photodetectors and thus a decrease in the quality of the signal [3, 5, 7]. The calculation of the CMRR in conventional 90° hybrid downconverters is well known [3] and, as established by the Optical Internetworking Forum (OIF) [12], it should be greater than 20 dB for all the operating spectrum band.

In 120° downconverters, there are not balanced detectors and the CMRR has to be defined. In particular, it should quantify the amplitude imbalances at the output electric signals (i.e. coupling mismatches, photodiode responsivities, amplitude imbalances due to phase diversity networks or electrical amplification) under illumination from the signal port. The CMRR in a 120° optical hybrid was previously theoretically proposed by us [7], being defined as:

$$CMRR_{120°\,downconverter} = 20\log_{10}\frac{A_{k3}i_3 + A_{k4}i_4 + A_{k5}i_5}{|A_{k3}|i_3 + |A_{k4}|i_4 + |A_{k5}|i_5} \quad (3)$$

where A_{kj} denotes the matrix coefficients to obtain the IQ components using the subscript j for the respective measured intensities (including the amplifiers, as shown in Fig.1), and k as the more restrictive value for either the I or the Q components. As it was theoretical and numerically demonstrated, the CMRR cancellation (in linear terms) would eliminate the detrimental interference to ideally perform colorless operation [7]. It should be noted that the matrix coefficients A_{kj} may refer to theoretical coefficients (2), which would lead to a theoretical CMRR, or calibrated coefficients that would lead to a calibrated CMRR function. Therefore, it is expected to obtain a much better colorless performance of the receiver when using the calibrated coefficients as they can be fitted to obtain a better CMRR cancellation.

III. Experimental Setup

Several experiments were carried out to evaluate the colorless performance of the receiver using both theoretical and calibrated matrix coefficients. The schematic setup and a photo of the InP based, integrated 2×3 optical hybrid downconverter are shown in Fig. 2. A CW tunable laser (TLS) operating in C and L bands with a linewidth of 25 kHz and a RIN of −145 dB/Hz is used both as the optical source for the transmitted signal and as the Local Oscillator (LO) in order to simplify the setup and focus on the benefits of the proposed receiver. This optical emitted signal is modulated by a 20 GHz bandwidth IQ modulator with a 50 Gbps, 12.5 Gbaud 16-QAM PRBS-9 signal that is generated using a 65 GSamples/s Arbitrary Wave Generator (AWG). The modulated signal is optically amplified with an EDFA to boost up the small output power of the IQ modulator and filtered with a 100 GHz @ 20 dB optical bandpass filter (OBPF). The received optical power is adjusted with a variable optical attenuator (VOA). The polarization of the received signal is controlled manually before it is injected in one of the fibers of a polarization-maintaining (PM) angled fiber array. The PM angled fiber array ensures the injection of the desired polarization and avoids back reflections at the end of the fiber and at the facet of the integrated receiver. The LO signal is also injected through a polarization maintaining fiber into another fiber of the array in such a way that both signal and LO present a TE mode, which is the design polarization for the optical chip. Both signals are then injected into the two input ports of the integrated coherent receiver using a six axis micro-positioning stage. The integrated 120° integrated optical receiver has been designed by us and fabricated in InP technology by Fraunhofer Heinrich-Hertz-Institute (HHI). More details about this receiver chip can be found in [13]. All the optical power values presented in this work are measured at the input of the PM fiber array, therefore the actual values injected into the chip will be about 1.5 dB lower due to insertion losses.

The three detected signals in the integrated 120° integrated optical receiver are amplified by three 26.5 GHz bandwidth amplifiers and captured using an 80 GSamples/s digital storage oscilloscope (DSO). These three digital signals are combined offline and digitally processed according to Section II to recover the transmitted symbols. The calibration coefficients are obtained by applying a linear calibration process to the three output photocurrents, including the electrical amplifiers, with a group of 512 known 16-QAM transmitted symbols at 12.5 GBd (50 Gbps). The result of this linear fit by least squares adjustments is the matrix M:

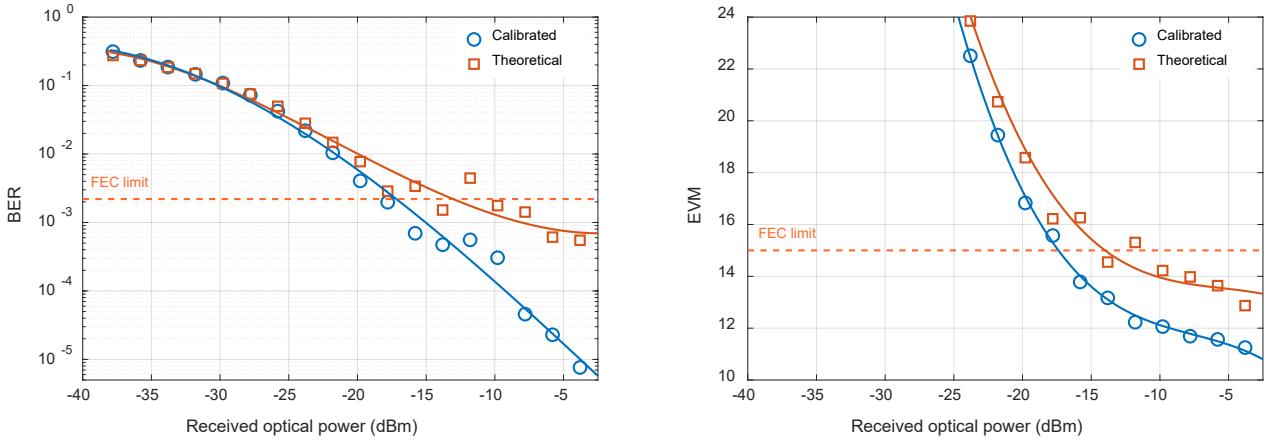

Fig. 3. BER (left) and EVM (right) vs received optical power just before injection at the integrated receiver for both theoretical and calibrated matrix coefficients.

$$\begin{bmatrix} i_3 \\ i_4 \\ i_5 \end{bmatrix} = \begin{bmatrix} a_3 & b_3 \\ a_4 & b_4 \\ a_5 & b_5 \end{bmatrix} \cdot \begin{bmatrix} I \\ Q \end{bmatrix} = \overline{\overline{M}} \cdot \begin{bmatrix} I \\ Q \end{bmatrix} \tag{4}$$

and the calibrated coefficients matrix (A) is obtained calculating the pseudoinverse of matrix M. The coefficients of the calibrated matrix may be very different from these of the theoretical one (2) because the receiver imbalances and any phase difference between LO and signal. This phase difference will rotate the calibrated matrix and hence the received constellation, but it can be corrected by the DFE and the symbols will be perfectly recovered. The calibrated coefficients matrix obtained with our setup at 1550nm, once this phase difference is corrected for a better comparison with the theoretical, is:

$$\overline{\overline{A}}_{\substack{Calibrated \\ coefficients}} = \begin{bmatrix} -0.53 & 0.86 & -0.47 \\ 0.90 & 0.00 & -0.91 \end{bmatrix} \tag{5}.$$

These calibrated coefficients are somewhat different from the theoretical coefficients (2), thus enabling correction of the received IQ constellation from the noticeable imbalances of the integrated receiver and the receiver RF components [11]. The main differences are a < 2º phase imbalance in the MMI branches, and a power imbalance (around 20%) in the central photodiode of the integrated receiver. These coefficients, although calculated at a single wavelength, can be used over a broad wavelength band to nearly cancel receiver imbalances, as it will be experimentally proven later. As we want to test the performance of the calibration process in the 2×3 integrated receiver, the IQ signals are obtained from the received signals by using both the theoretical 120° transfer matrix (2) and the calibrated matrix at 1550 nm (5). Therefore, we will use two IQ signals (theoretical and calibrated) obtained from the same captured currents to compare the performance of the calibration process. Both signals are clock recovered and equally processed by a decision-directed phase locked loop (DDPLL) to correct the frequency and phase error offsets and a decision feedback equalizer (DFE) for ISI cancelation [14]. Finally, the BER and the Error Vector Magnitude (EVM) of the symbols from the center of the theoretical symbols in the constellation, normalized by the average power, are calculated. As reference, it has been considered a BER limit of 2.2×10^{-3} (for enhanced forward error correction (E-FEC) coding with 7% redundancy overhead [15]), which corresponds approximately to an EVM of 15% for 16-QAM modulation [16].

An adjacent wavelength channel will be also introduced in the 120° integrated coherent receiver to evaluate its interfering rejection capability. Light emitted from another TLS is modulated using a Mach-Zehnder modulator with a 12.5 Gbaud OOK signal (with similar extinction ratio than a 16-QAM signal) obtained from a pseudorandom pattern generator (PPG). Its polarization is manually controlled and it is combined with the signal using a PM coupler as can also be seen in Fig. 2. The setup is configured so the interfering signal presents the same polarization state than the signal and LO in the integrated device to avoid random polarization dependent losses and to achieve the worst possible interference situation.

IV. Results and Discussion

The performance of the 120° integrated downconverter at the design wavelength of 1550 nm can be appreciated in Fig. 3, where BER and EVM are plotted versus the received signal power for the symbols demodulated with theoretical and calibrated coefficients. It should be noted that all the depicted values are obtained from the same set of three currents measured for each received optical power. Efficient compensation of hardware impairments can only be achieved with calibrated coefficients as it is confirmed by the continuous reduction of BER as the signal power increases. On the contrary, when using theoretical coefficients, the function BER will cease to decrease once the uncancelled signal power-dependent self-beating interference term will be imposed. In our experimental work, due to the limitation in the maximum optical signal power, it could only be partially seen. In this way, the receiver with theoretical coefficients will be reduced its dynamic range and suffer a sensitivity penalty (considering the E-FEC BER limit) of 4.1 dB compared to the receiver with calibrated coefficients. Regarding the EVM, it is always lower

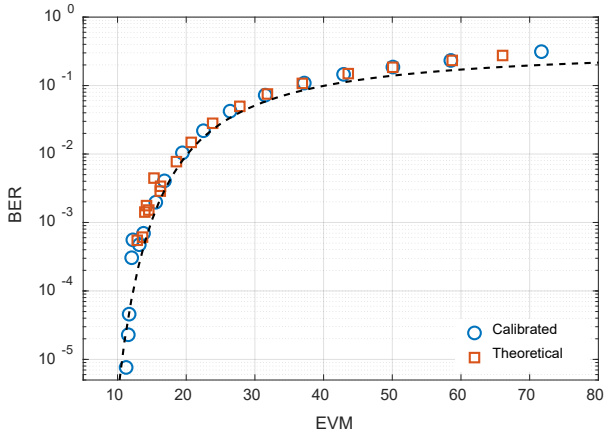

Fig. 4. Experimental BER versus measured EVM for calibrated and theoretical coefficients. The dashed line represents the theoretical prediction (6).

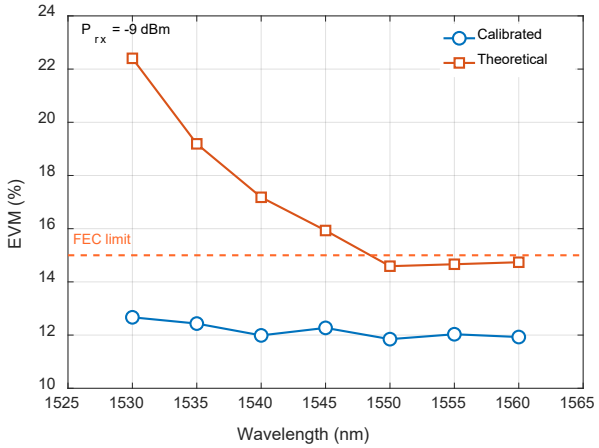

Fig. 5. EVM measurements in function of the received signal wavelength using theoretical and calibrated coefficients in the C-band for a received signal power of -9 dBm.

for calibrated coefficients (around two percentage points below) especially for optical powers above -15 dBm.

In an ideal coherent receiver limited by optical and electrical additive white gaussian noise (AWGN), the BER can be analytically related to the EVM obtained from the received M-QAM constellation according to [16]:

$$BER \approx 2\frac{1-M^{-1/2}}{\log_2 M} erfc\left(\sqrt{\frac{3}{2}\cdot\frac{1}{(M-1)\cdot EVM^2}}\right). \quad (6)$$

where M is the modulation order (M=16) and *erfc* is the complementary error function. This theoretical relation can be combined with the experimental values of Fig. 3 as is done in Fig. 4_new, which shows a comparison between the measured BER versus EVM and the theoretical curve (6). It is clearly shown that measured values of the calibrated receiver are in close agreement with the expected performance of an ideal receiver. Also, as previously shown in Fig.3, it is evident clear that measured performance of the un-calibrated (theoretical coefficients) receiver fails to reach the ideal performance in the low BER regime corresponding to high input signal power. Please notice that these measurements, although not assessing the total receiver sensitivity, which could be far from the ideal due to power losses or excess noise into the experimental setup, clearly show that calibrated receiver is performing as a well-behaved theoretical receiver perturbed by AWGN.

In the following measurements a signal optical power of -9 dBm will be used because it achieves, for both theoretical and calibrated coefficients, an error below the E-FEC limit.

Fig. 5 depicts the EVM obtained when the signal wavelength (and consequently the LO wavelength) is varied within the amplified C-band (1530 nm – 1565 nm). It can be seen that an efficient operation in a wideband spectrum can only be achieved using calibrated coefficients, which were obtained at the design wavelength of 1550 nm. Fig. 5 shows a constant EVM result of about 12% when using calibrated coefficients, while theoretical coefficients produce worse results due to uncompensated amplitude and phase imbalances, with a minimum EVM of 14.5%. EVM results with theoretical coefficients are below the FEC limit in a reduced range of about 10 nm, from 1550 to 1560nm, so its bandwidth is clearly narrowed.

This behavior is confirmed by the measurements shown in Fig. 6, where demodulated 16-QAM constellations are depicted at the lower (1530 nm) and central wavelengths (1550 nm) of the C-band. It can be clearly seen how constellations cannot be adequately recovered with theoretical coefficients, producing

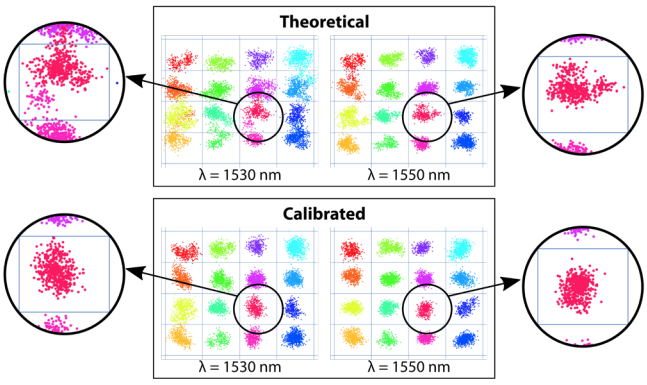

Fig. 6. Reconstructed 16-QAM constellations for a signal power of -9 dBm using theoretical (up) and calibrated (down) coefficients at 1530 nm and 1550 nm. Ideal decision boundaries are illustrated.

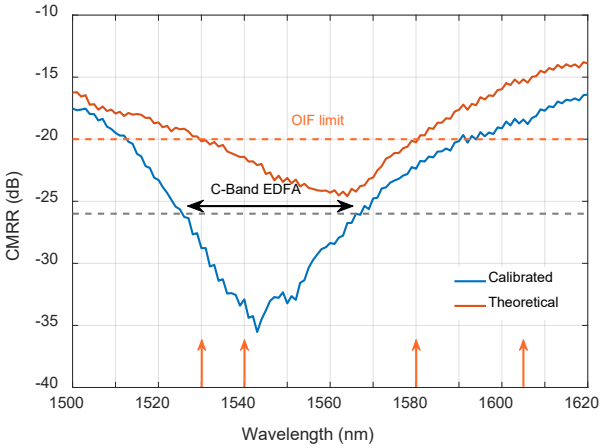

Fig. 7. Measured CMRR for theoretical and calibrated coefficients. Arrows indicate the interfering signals that have been tested in the last part of the paper.

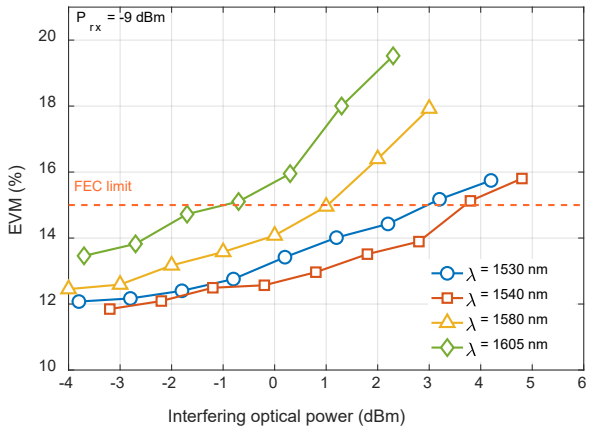

Fig. 8. EVM receiver performance for calibrated coefficients versus the received interfering signal power for different values of the interfering wavelength (received signal power is maintained at -9 dBm).

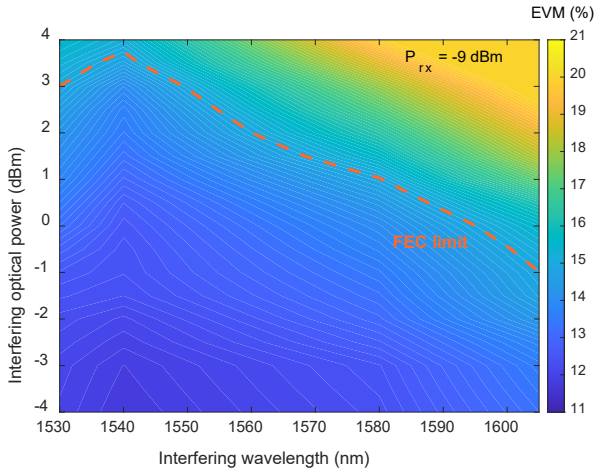

Fig. 9. EVM receiver performance for calibrated coefficients versus the interference wavelength and received interfering power (received signal power is maintained at -9 dBm).

symbols out of the decision boundaries and thus causing a higher BER and EVM. On the other hand, a single set of calibrated coefficients can better resolve undistorted constellations in a wider spectrum. Furthermore, as can be seen in the insets of Fig 6, the shape of cloud of points of each received symbol with theoretical coefficients is clearly distorted and irregular in contrast to the circular-like (Gaussian) shape of the constellation cloud obtained with calibrated coefficients.

As we stated in Section 2, the CMRR provides a figure of merit of the colorless performance of a coherent receiver. Certainly, the interference rejection at a specific wavelength will be high if the receiver shows a reduced amplitude imbalance and, therefore, a high CMRR. Fig. 7 represents the wavelength dependence of the theoretical and calibrated CMRR for the proposed 120° coherent receiver obtained as in (3) from theoretical and calibrated matrix coefficients. It is important to clarify here that the depicted CMRRs are obtained from the currents obtained by the receiver and the external amplifiers. From Fig. 7 it can be clearly seen that the receiver with calibrated coefficients achieves a much better CMRR, well below -25 dB in the C-band, and therefore should be much less sensitive to interfering wavelength channels than the theoretical CMRR. As it refers to the noise performance, it should also be expected a high common-mode noise rejection from the high CMRR provided by the calibrated receiver in the operation band. This receiver, calibrated at 1550 nm, should operate on a wide operating band (equivalent to C+L band) as its CMRR fulfills the OIF -20 dB restriction on an 80 nm range. However, the required optical amplification of the modulated signal provided by the EDFA in our set-up limited the signal operation to the C-band. It is worth to note that this significant broadband improvement of the measured CMRR has been achieved using the calibration coefficients obtained at a single wavelength of 1550nm, thus confirming experimentally the proposed technique.

The colorless performance of the receiver has also been analyzed from the EVM and BER measurements in the presence of an interfering signal in several wavelengths (indicated as arrows in Fig. 7). Please note that the receiver interference rejection makes no sense if, as Fig. 5 stated for the received signal with theoretical coefficients, the uncompensated phase and amplitude receiver imbalances could not even allow single channel signal reception in the operation C-band. For this reason, in the following the study of the receiver colorless performance will be limited to the use of calibrated coefficients. Since a phase modulated signal has no significant amplitude variations and, therefore, power changes are not substantial, using it as an interfering signal would barely distort the received signal. Hence, as is depicted in the setup of Fig. 2, we have used amplitude modulated interfering signals (OOK) with an extinction ratio similar to the 16-QAM signals to analyze the interference on the coherent reception. The test signal is a 50 Gbps 16-QAM signal at 1550 nm and its received optical power is maintained at -9 dBm which, as can be seen in Fig. 3 and Fig. 5, exhibited in absence of interference an EVM value of about 12% and a BER well below the FEC limit.

Figs. 8 and 9 represent, for the calibrated 120° coherent receiver, EVM measurements versus the interfering optical power and interfering wavelength. It must be noticed that the interference contribution will be weighted by its power and the CMRR at its respective wavelength [7].

Therefore, as is clearly seen in Fig. 8, the EVM function versus the interfering power will show a flatter slope at the interference wavelengths where the receiver achieves a better CMRR. Thus, attending the enhanced interference rejection provided by the high CMRR shown in Fig. 7 for the C-band, the main limitation will be imposed by the interference located out of this band, as experimentally confirmed for 1580 nm and, especially, for 1605 nm. As pointed in Fig. 9, there will be a maximum admissible interfering power of nearly 2 dBm to assure an EVM below the FEC limit in the complete C-band (1530-1565 nm). This represents a very strong channel interference immunity, close to 11 dB above the signal level. Although a precise evaluation of the number of interfering channels supported by the calibrated receiver cannot be done with our measurement setup, a lower-limit estimation can be

done in a worst-case scenario: 12 interfering channels with the same optical power than received signal, entering the receiver with identical polarization state and time alignment. In a realistic situation the number of supported interferent channels will be arguably higher, since a strong single interfering channel induces much more penalty than the same interferent power distributed on various interfering WDM channels [2].

V. Conclusions

In this work, we have shown the performance of an integrated InP 120° coherent receiver using 50 Gbps 16-QAM channels. Hardware impairments due to the fabrication process can be partially compensated, without extra computational cost, through a set of calibrated matrix coefficients in order to improve the constellation reconstruction and so, reduce the bit error rate. The experimental results in terms of BER and EVM show that the use of calibrated coefficients in the IQ reconstruction matrix provides a better performance than using theoretical coefficients and a wider operating band. Moreover, the calibration can be applied using analog electronics and thus reducing DSP workload and improving energy efficiency. It has been shown that calibration also improves the CMRR behavior of the device on a wideband spectrum achieving a better interfering signal rejection without using any kind of optical filtering, which reduces the operational cost of the communication system. This confirms a remarkable colorless behavior of our calibrated 2×3 integrated coherent receiver in the C-band operation. Therefore, digital coherent reception predicted for the next generation of optical metro and access networks could benefit from the features experimentally assessed for the proposed receiver.

References

[1] S. Tibuleac and M. Filer, "Transmission Impairments in DWDM Networks With Reconfigurable Optical Add-Drop Multiplexers," J. Lightw. Technol., vol. 28, no. 4, pp. 557-598, Feb.15, 2010.

[2] L. E. Nelson et al., "Detection of a Single 40 Gb/s Polarization-Multiplexed QPSK Channel With a Real-Time Intradyne Receiver in the Presence of Multiple Coincident WDM Channels," J. Lightw. Technol., vol. 28, no. 20, pp. 2933-2943, Oct.15, 2010.

[3] B. Zhang, C. Malouin, and T. J. Schmidt, "Towards full band colorless reception with coherent balanced receivers," *Opt. Express*, vol. 20, no. 9, pp. 10339-10352, Apr. 2012.

[4] Y. Painchaud, M. Poulin, M. Morin, and M. Têtu, "Performance of balanced detection in a coherent receiver," *Opt. Express*, vol. 17, no. 5, pp. 3659-3672, Mar. 2009.

[5] I. Fatadin, S. J. Savory and D. Ives, "Compensation of Quadrature Imbalance in an Optical QPSK Coherent Receiver," *IEEE Photon. Technol. Lett.*, vol. 20, no. 20, pp. 1733-1735, Oct. 2008.

[6] P. J. Reyes-Iglesias, I. Molina-Fernández, A. Moscoso-Mártir, and A. Ortega-Moñux, "High-performance monolithically integrated 120° downconverter with relaxed hardware constraints," *Opt. Express*, vol. 20, no. 5, pp. 5725-5741, Feb. 2012.

[7] P. J. Reyes-Iglesias, A. Ortega-Moñux, and I. Molina-Fernández, "Colorless monolithically integrated 120° downconverter," *Opt. Express*, vol. 21, no. 20, pp. 23048-23057, Oct. 2013.

[8] C. Xie *et al.*, "Colorless coherent receiver using 3x3 coupler hybrids and single-ended detection," *Opt. Express*, vol. 20, no. 2, pp. 1164-1171, Jan. 2012.

[9] P. Dong, C. Xie, and L. L. Buhl, "Monolithic polarization diversity coherent receiver based on 120-degree optical hybrids on silicon," *Opt. Express*, vol. 22, no. 2, pp. 2119-2125, Jan. 2014.

[10] F. M. Ghannouchi and R. G. Bosisio, "An alternative explicit six-port matrix calibration formalism using five standards," *IEEE Trans. Microw. Theory Tech.*, vol. 36, no. 3, pp. 494–498, Mar. 1988.

[11] P. J. Reyes-Iglesias, A. Ortega-Moñux, and I. Molina-Fernández, "Enhanced monolithically integrated coherent 120° downconverter with high fabrication yield," *Opt. Express*, vol. 20, no. 21, pp. 23013-23018, Oct. 2012.

[12] *Implementation Agreement for Integrated Dual Polarization Intradyne Coherent Receivers*, OIF-DPC-RX-01.2, Optical Internetworking Forum (OIF), Nov. 2013. [Online]. Available: www.oiforum.com/technical-work/implementation-agreements-ias

[13] P Runge *et al.*, "Monolithic integrated InP receiver chip for coherent phase sensitive detection in the C-and L-band for colorless WDM applications", in *2014 European Conference on Optical Communication (ECOC)*, Cannes, France, 2014.

[14] J. Clemente *et al.*, "Experimental Demonstration of Colorless Operation of an Integrated 120° Coherent Receiver", in *2018 European Conference on Optical Communication (ECOC)*, Rome, Italy, 2018.

[15] *Forward error correction for high bit-rate DWDM submarine systems*, Rec. ITU-T G.975.1, International Telecommunications Union, Geneva, Switzerland, Feb. 2014.

[16] R. Schmogrow *et al.*, "Error Vector Magnitude as a Performance Measure for Advanced Modulation Formats," *IEEE Photon. Technol. Lett.*, vol. 24, no. 1, pp. 61-63, Jan. 2012.